Regulation of quantal shape by Rab3A: evidence for a fusion pore-dependent mechanism

Xueyong Wang[1,2], Ramachandran Thiagarajan[1,2], Qingbo Wang[1,2], Teclemichael Tewolde[1], Mark M. Rich[1,2] and Kathrin L. Engisch[1,2]

[1]*Department of Physiology, Emory University School of Medicine, Atlanta, GA 30322, USA*
[2]*Department of Neuroscience, Cell Biology and Physiology, Boonshoft School of Medicine, Wright State University, Dayton, OH 45435, USA*

The function of Rab3A, a small GTPase located on synaptic vesicles, is not well understood. Studies in the Rab3A$^{-/-}$ mouse support a role in activity-dependent plasticity, but have not reported any effects on spontaneously occurring miniature synaptic currents, except that there is a decrease in resting frequency at the neuromuscular junction. Therefore we were surprised to find an increase in the occurrence of mEPCs with abnormally long half-widths at the neuromuscular junctions of Rab3A$^{-/-}$ mice. The abnormal miniature endplate currents (mEPCs), which have significantly greater charge than the average mEPCs for the same fibres, could arise from larger vesicles. However, the type of mEPC most increased in Rab3A$^{-/-}$ mice has a slow rise, which suggests it is not the result of full collapse fusion. To test if the slow mEPCs increased after loss of Rab3A could be due to malfunctioning fusion pores, we used carbon fibre amperometry to record pre-spike feet, which have been shown to correspond to the initial opening of a narrow fusion pore, in adrenal chromaffin cells of wild-type and Rab3A$^{-/-}$ mice. We found that small amplitude pre-spike feet with abnormally long durations were increased in Rab3A$^{-/-}$ cells. The correspondence between mEPC and amperometric data supports our interpretation that slow rising, long half-width mEPCs are caused by reduced diameter fusion pores that remain open longer. These data could be explained by a direct action of Rab3A on the fusion pore, or by Rab3A-dependent control of vesicles with unusual fusion pore characteristics.

(Received 15 January 2008; accepted after revision 20 June 2008; first published online 26 June 2008)
Corresponding author K. Engisch: Department of Neuroscience, Cell Biology and Physiology, 014 M&M Building, Boonshoft School of Medicine, Wright State University, 3640 Colonel Glenn Hwy., Dayton, OH 45435, USA. Email: kathrin.engisch@wright.edu

Rab3A is a member of a family of small GTPases associated with vesicles of cells with a regulated secretory pathway (Darchen *et al.* 1990; Fischer von Mollard *et al.* 1990; Regazzi *et al.* 1992). Since deletion of several Rab GTPases in yeast caused defects in growth, vesicle fusion and/or protein transport (Salminen & Novick, 1987; Segev & Botstein, 1987; Wichmann *et al.* 1992), it was surprising that the Rab3A$^{-/-}$ mouse was viable and fertile, with no apparent deficits in synaptic transmission (Geppert *et al.* 1994). One explanation for the lack of dramatic effects is the presence of three other closely related family members. The quadruple Rab3ABCD$^{-/-}$ mouse was recently produced, and it dies shortly after birth (Schluter *et al.* 2004). However, synaptic currents evoked in hippocampal neurons cultured from embryonic Rab3ABCD$^{-/-}$ mice are only reduced 50%. These results indicate that Rab3 proteins are not essential for synaptic vesicle fusion.

Despite normal evoked transmitter release in Rab3A$^{-/-}$ mice, there are changes in vesicle transport and fusion. Stimulation-dependent movement of vesicles toward the membrane is reduced in hippocampal synaptosomes of Rab3A$^{-/-}$ mice (Leenders *et al.* 2001), and there are fewer docked vesicles at the neuromuscular junction of Rab3A$^{-/-}$ mice (Coleman *et al.* 2007). Furthermore, physiological experiments indicate that Rab3A is important for plasticity of vesicle fusion. A presynaptic form of long-term potentiation is abolished in the Rab3A$^{-/-}$ mouse (Castillo *et al.* 1997; Huang *et al.* 2005). Increased frequency of miniature synaptic currents induced by neurotrophin application is reduced (Thakker-Varia *et al.* 2001; Alder *et al.* 2005). Finally, short-term facilitation during repetitive stimulus trains is increased in Rab3A$^{-/-}$ and Rab3ABCD$^{-/-}$ mice (Hirsh

X. Wand and R. Thiagarajan contributed equally to this work.

 DOI: 10.1113/jphysiol.2008.151191

et al. 2002; Schoch *et al.* 2002; Schluter *et al.* 2004). Taken together, these data suggest that Rab3A plays a role in controlling the number of available vesicles, likely in an activity-dependent manner.

None of the previous observations at synapses of $Rab3A^{-/-}$ or $Rab3ABCD^{-/-}$ mice indicated that Rab3A deletion would have an effect on the shape of a single quantum. However, we find that the incidence of rare miniature endplate currents with abnormal properties, such as long half-widths, and slow rises, was increased at neuromuscular junctions of $Rab3A^{-/-}$ mice. We hypothesized that the absence of Rab3A leads to a greater probability of malfunctioning fusion pores with small diameters and prolonged open times. Our interpretation is supported by data from carbon fibre amperometric current recordings of pre-spike feet in adrenal chromaffin cells of wild-type and $Rab3A^{-/-}$ mice.

Methods

Animals

$Rab3A^{+/+}$ and $Rab3A^{-/-}$ mice were obtained from mating $Rab3A^{+/-}$ mice. $Rab3A^{+/-}$ breeder pairs were provided by M. Bucan (University of Pennsylvania) and bred at Emory University and Wright State University. $Rab3A^{-/-}$ mice were originally derived from C57BL/6J, 129Sv-$Rab3A^{tmSud}$, stock code 002443 from Jackson Laboratory, and backcrossed for three generations to C57BL/6J (N4) (Kapfhamer *et al.* 2002). $Rab3A^{+/+}$, $Rab3A^{+/-}$ and $Rab3A^{-/-}$ mice were genotyped by microsatellite marker D8Mit31. Prior to tissue removal, animals were killed by CO_2 inhalation according to protocols approved by the Institutional Animal Care and Use Committee of Emory University, and the Laboratory Animal Care and Use Committee of Wright State University.

Chromaffin cell culture

Cultures were prepared from 4 to 6 glands obtained from animals of the same sex and genotype. Medullae were isolated using a scalpel blade, incubated with stirring at 37°C in a calcium- and magnesium-free phosphate buffer, adjusted to 320 mosmol l^{-1} (Fulop & Smith, 2006) and containing 0.033% collagenase type 2 (Worthington, Lakewood, NJ, USA). Glands were triturated at periodic intervals for a total digest time of 30 min. Cells were centrifuged at 1100 r.p.m. and plated in Dulbecco's modified Eagle's medium (DMEM) containing 10% fetal bovine serum, antibiotics, and mitotic inhibitors on glass coverslips coated with a 1 : 12 dilution of Matrigel (BD Biosciences, San Jose, CA, USA). Recordings were performed at room temperature, 24 h after plating.

Neuromuscular junction recording

The tibialis anterior muscle was dissected, partially bisected and pinned to a Sylgard-coated recording dish, and perfused with (in mM): 118 NaCl, 3.45 KCl, 11 dextrose, 26.2 $NaHCO_3$, 1.7 NaH_2PO_4, 0.7 $MgSO_4$, 2 $CaCl_2$, bubbled with 5% CO_2–95% O_2. Muscle fibres were stained with 10 μM 4-(4-diethylaminostyryl)-*N*-methylpyridinium iodide (4-Di-2ASP; Invitrogen, Carlsbad, CA, USA) (Magrassi *et al.* 1987) and imaged with a Leica DMR upright epifluorescence microscope to allow visualization of surface nerve terminals as well as individual muscle fibres. Prior to experiments, the muscle fibres were crushed at a point far from the endplate band to prevent muscle contraction because in some recordings we also stimulated the nerve (data not shown). Fibres were impaled with two microelectrodes within 100 μm of the endplate and voltage clamped to −45 mV. Spontaneously occurring miniature endplate currents were recorded at room temperature with a Geneclamp 500B (Molecular Devices, Sunnyvale, CA, USA) and acquired with custom software written by Martin Pinter (Emory University).

Amperometry

A coverslip containing chromaffin cells was transferred to a glass bottom recording chamber and perfused with extracellular solution containing (in mM): 130 NaCl, 2 KCl, 10 dextrose, 10 Na-Hepes, 1 $MgCl_2$, 5 $CaCl_2$, 5 *N*-methyl-D-glucamine, pH 7.2. Amperometric events stimulated by 8 min of exposure to 25 mM K^+ solution (25 mM NaCl replaced with 25 mM KCl) were recorded with an 8 μm carbon fibre microelectrode (Thiagarajan *et al.* 2004) connected to a HEKA EPC-10 patch clamp amplifier connected to a computer running Patchmaster software (HEKA Elektronik, Lambrecht/Pfalz, Germany). Electrode potential was +780 mV. Data were sampled at 20 kHz and filtered at 2.9 kHz.

Data analysis

Miniature endplate currents were detected, aligned and analysed with custom software written by Martin Pinter (Emory University). Frequency histograms and Gaussian fits were generated with custom macro routines in Excel. Outliers were values above the $y = 0.05$ point on the right side of the Gaussian. Unless otherwise noted, for each parameter a mean value was obtained for every fibre, and data compared across animals with nested analysis of variance.

Amperometric currents were detected, aligned and analysed using the Quantal Analysis macro written for Igor Pro software (Wavemetrics, Lake Oswego, OR, USA) by Eugene Mosharov (Mosharov & Sulzer, 2005). Data were

smoothed with a 1526 Hz Gaussian filter prior to analysis. Amperometric spikes < 10 pA were not included.

Data were compared by Student's *t* test, Mann–Whitney *U* test, or Kolmogorov–Smirnov statistics, as indicated. Data are presented as means ± S.E.M.

Results

Increased occurrence of abnormal mEPCs with long half-widths at the neuromuscular junctions of Rab3A$^{-/-}$ mice

Spontaneously occurring miniature endplate currents (mEPCs) were recorded from the tibialis anterior neuromuscular junction under two-electrode voltage clamp. Figure 1*A* shows selected traces recorded in a wild-type fibre. The majority of mEPCs have a fast rise, an exponential decay and moderate amplitude. There is also one event with an abnormally large amplitude and long duration (*). The abnormal event represents ∼1% of the mEPCs recorded in the fibre, as illustrated by an overlay of 100 mEPCs in Fig. 1*C*. Selected traces recorded in a fibre from a Rab3A$^{-/-}$ animal are shown in Fig. 1*B*. There are two abnormal events (*), and an overlay of 100 mEPCs from this fibre (Fig. 1*D*) indicates that such events comprised > 1% of the total.

The amplitude–frequency distributions for the wild-type and Rab3A$^{-/-}$ fibres are shown in Fig. 1*E* and *F*, respectively, and half-width frequency distributions in Fig. 1*G* and *H*. We quantitatively identified an 'abnormal' mEPC as an event with an amplitude or a half-width that was outside the $y = 0.05$ value of a Gaussian fit to the frequency distribution. These outliers are highlighted in red. For the wild-type fibre, the abnormal event was an outlier on both the amplitude and half-width frequency distributions. For the Rab3A$^{-/-}$ fibre, there were three amplitude outliers and five half-width outliers. The frequency distributions of percentage half-width outliers for 149 fibres from seven wild-type animals, and 125 fibres from six Rab3A$^{-/-}$ animals are shown in Fig. 2*A* and *B*, respectively. Comparison of the cumulative distributions is shown in Fig. 2*C*. Over 75% of wild-type fibres have < 2% of half-width outliers (114/149), whereas only 53% of Rab3A$^{-/-}$ fibres have < 2% (66/125). Almost 10% of Rab3A$^{-/-}$ fibres have over 8% of half-width outliers (12/125); for wild-type fibres only 1 out of 149 had above 8%. The variance was significantly increased in Rab3A$^{-/-}$ data (variance, wild-type, 3.34, Rab3A$^{-/-}$, 10.28, $F_{max} = 3.08$, $P < 0.01$), as was the mean (2.59% ± 0.52 *versus* wild type, 1.31 ± 0.09%, $P < 0.001$, Mann–Whitney *U* test on fibres; $P < 0.0001$, Kolmogorov–Smirnov; $P = 0.017$, ANOVA, 7 wild-type and 6 Rab3A$^{-/-}$ animals). The effect of Rab3A loss was specific for half-width outliers. The distribution for amplitude outliers was not altered in Rab3A$^{-/-}$ mice (not shown), and the mean percentages were not different (wild-type, 1.61 ± 0.18% *versus* Rab3A$^{-/-}$, 1.80 ± 0.15%, $P = 0.42$, Mann–Whitney *U* test; $P = 0.44$, ANOVA). Although loss of Rab3A had no effect on the percentage of amplitude outliers, there was an increase in events for which both the amplitude and the half-width were outliers (wild-type, 0.21 ± 0.05% *versus* Rab3A$^{-/-}$, 0.61 ± 0.14%, $P = 0.02$). Loss of Rab3A had no effect on overall mean amplitude or mean half-width (amplitude, wild-type, 1.27 ± 0.02 nA *versus* Rab3A$^{-/-}$, 1.28 ± 0.02 nA, $P = 0.96$; half-width, wild-type, 1.04 ± 0.01 ms *versus* Rab3A$^{-/-}$, 1.08 ± 0.01 ms, $P = 0.44$, ANOVA).

A decrease in frequency of normal mEPCs has been reported at the soleus and diaphragm neuromuscular junctions of Rab3A$^{-/-}$ mice (Sons & Plomp, 2006; Coleman *et al.* 2007). This alone, with no change in frequency of abnormal mEPCs, could result in an increase in the percentage of mEPCs that are abnormal. Initially, we found that the difference in mean mEPC frequency between wild-type and Rab3A$^{-/-}$ animals did not reach significance (wild-type, 2.56 ± 0.37 s^{-1} *versus* Rab3A$^{-/-}$, 1.54 ± 0.41 s^{-1}, $P = 0.17$, ANOVA). However, a small number of fibres had extremely high frequencies, which may indicate damage and/or an increase in intracellular calcium. When fibres with mEPC frequencies ≥ 5 s^{-1} were removed, we found a significant decrease in normal mEPC frequency in Rab3A$^{-/-}$ fibres as previously observed (wild-type, 1.32 ± 0.07 s^{-1} *versus* Rab3A$^{-/-}$, 1.03 ± 0.07 s^{-1}, $P = 0.024$, ANOVA). Although the decrease in normal mEPC frequency contributed to the increased percentage of mEPCs with abnormal half-width in Rab3A$^{-/-}$ animals, the frequency of abnormal half-width mEPCs was also significantly increased (wild-type, 0.015 ± 0.003 s^{-1} *versus* Rab3A$^{-/-}$, 0.025 ± 0.003 s^{-1}, $P = 0.045$, ANOVA).

To further understand what mechanism causes a mEPC with an excessively long half-width, we visually examined all events identified as half-width outliers. Figure 3 shows individual mEPCs selected from the recording of the Rab3A$^{-/-}$ fibre described in Fig. 1. The first mEPC (*a*) is 'normal': it closely follows the red trace, produced by averaging all the mEPCs from that fibre. The other three mEPCs (*b*, *c* and *d*) are 'abnormal'. The abnormal mEPCs clearly have a larger charge than the average mEPC. To determine if this was generally true, we compared the total charge for mEPCs with abnormal half-widths to that of the average mEPC for the same fibre. We limited the analysis to those fibres with at least five abnormal half-width mEPCs, and determined the mean value for comparison to the charge for the average mEPC trace (created by averaging all the traces for the fibre). For wild-type fibres and Rab3A$^{-/-}$ fibres, the total charge for abnormal half-width mEPCs was significantly increased over that of the average mEPC (wild-type, average mEPC, 1.7 ± 0.1 pC; wild-type, abnormal half-width mEPC, 3.1 ± 0.4 pC; $n = 8$ fibres,

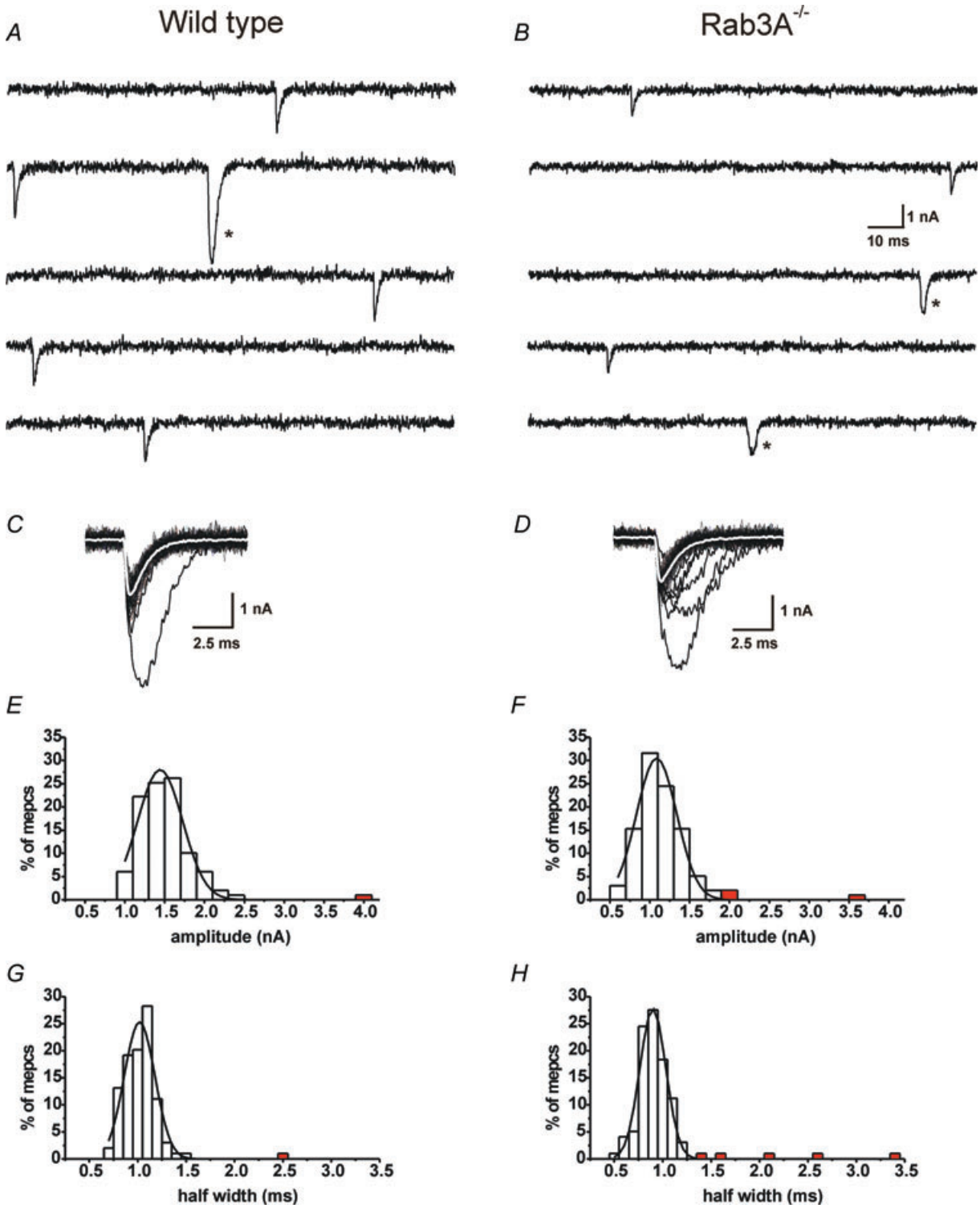

Figure 1. Abnormal miniature endplate currents (mEPCs) at the neuromuscular junctions of wild-type and Rab3A$^{-/-}$ mice

A and *B*, selected 125 ms records of spontaneously occurring mEPCs in a wild-type fibre and Rab3A$^{-/-}$ fibre, respectively. Records were chosen to illustrate shapes of normal and 'abnormal' (*) events, and were separated by 1 or more records without events. *C* and *D*, overlays of 100 aligned mEPCs from the wild-type and Rab3A$^{-/-}$ fibres in *A* and *B*. The white traces are the averages of the aligned mEPCs. *E* and *F*, frequency histograms of amplitudes, and *G* and *H*, frequency histograms of half-widths, for wild-type and Rab3A$^{-/-}$ fibres from *A* and *B*. Outliers, shown in red, are defined by being outside the $y = 0.05$ value of the Gaussian fit (smooth line).

$P < 0.005$; Rab3A$^{-/-}$, average mEPC, 1.6 ± 0.1 pC; Rab3A$^{-/-}$, abnormal mEPC, 3.8 ± 0.3 pC, $n = 19$ fibres, $P < 0.0001$; paired t tests).

The abnormal mEPCs are 'abnormal' in different ways. Traces *b* and *c* initially follow the average trace, and reach their peak with 10–90% rise times > 0.65 ms, compared to ~0.2 ms for the average trace. Trace *d* rises more slowly than the average trace from its onset, with a 10–90 rise time of 1.0 ms. What mechanism could produce mEPCs with larger charges and delayed peaks? At the neuromuscular junction, neurotransmitter release is thought to be an all or none event in which full fusion of the synaptic vesicle leads to instantaneous release of its entire contents (Kuffler & Yoshikami, 1975; Heuser *et al.* 1979; Miledi *et al.* 1982; Becherer *et al.* 2001; Dickman *et al.* 2005). If full fusion is assumed, events with a larger total charge must be due to (1) increased vesicular concentration of transmitter; (2) increased size of the vesicle; or (3) compound fusion of multiple vesicles. Events with a normal half-width and abnormally large amplitude might be caused by increased vesicular transmitter concentration, but these events were not increased in Rab3A$^{-/-}$ animals. Events with a wider half-width but normal rising phase can be explained by fusion of a larger vesicle or multiple vesicles. While it is possible that slow rising mEPCs might arise from vesicles that fuse at a greater distance from the receptors, or at a site that contains fewer receptors, such events should produce a smaller total charge, not a larger one. Therefore slow rising mEPCs are difficult to explain by a full fusion mechanism. We set out to determine which type of abnormal mEPC was increased in the absence of Rab3A.

We subclassified mEPCs identified as outliers on the half-width frequency histogram into three groups: I, mEPCs with initial time courses that match that of the average trace (Fig. 4*A*); II, mEPCs with initial time courses that match the average trace but continue to rise to a delayed peak (Fig. 4*B*); and III, mEPCs with slow rises to delayed peaks (Fig. 4*C*). In categories with delayed peaks (II and III), we included only mEPCs with a 10–90% rise time of ≥ 0.65 ms. We found that events in category I were not increased in Rab3A$^{-/-}$ animals (Table 1). In contrast, events with altered time courses, categories II and III, were increased 1.9-fold and 3.5-fold, respectively, in recordings from Rab3A$^{-/-}$ animals. These data are consistent with the idea that loss of Rab3A may cause an increase in the fusion of large vesicles or multiple vesicles (category II), and an increase in fusion events with altered kinetics (category III). To test the idea that loss of Rab3A affects fusion pore kinetics, we turned to another preparation in which the characteristics of release through a fusion pore can be examined: carbon fibre amperometry recording of catecholamine release from adrenal chromaffin cells.

Increased occurrence of amperometric spikes with small amplitude, long duration pre-spike feet in adrenal chromaffin cells of Rab3A$^{-/-}$ mice

A carbon fibre held at a large positive potential can oxidize catecholamines released during fusion of large dense cored vesicles in adrenal chromaffin cells (Wightman *et al.* 1991). The electrons generated by the oxidation are detected as a spike of amperometric current. Some currents have a pre-spike foot, a small amplitude current that immediately precedes the spike (Chow *et al.* 1992). Simultaneous admittance and amperometric measurements have shown that the pre-spike foot corresponds to the opening of a narrow fusion pore (Albillos *et al.* 1997). If the changes we observe in mEPCs are due to altered fusion

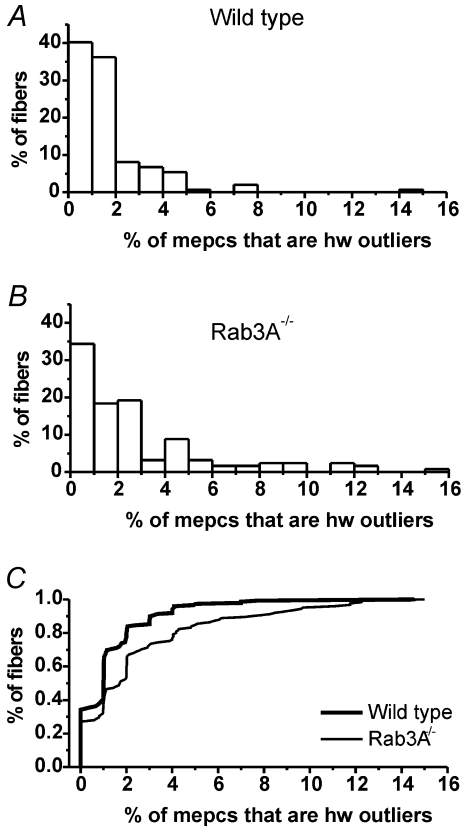

Figure 2. Fibres have higher percentages of mEPCs that qualify as half-width outliers in Rab3A$^{-/-}$ animals
A and *B*, frequency histograms for percentage of mEPCs that are half-width outliers, for wild-type fibres and Rab3A$^{-/-}$ fibres, respectively. *C*, cumulative plots for the same data in *A* and *B*. For each fibre, the percentage of half-width outliers was determined by counting the number of mEPCs with values greater than the $y = 0.05$ point on the Gaussian fit of the half-width frequency histogram, dividing by the total number of mEPCs, and multiplying by 100. The two groups are statistically different, $P < 0.001$, Mann–Whitney U test on fibres; $P < 0.001$, Kolmogorov–Smirnov on fibres; $P = 0.017$, ANOVA on animals. 149 fibres from 7 wild-type animals; 125 fibres from 6 Rab3A$^{-/-}$ animals.

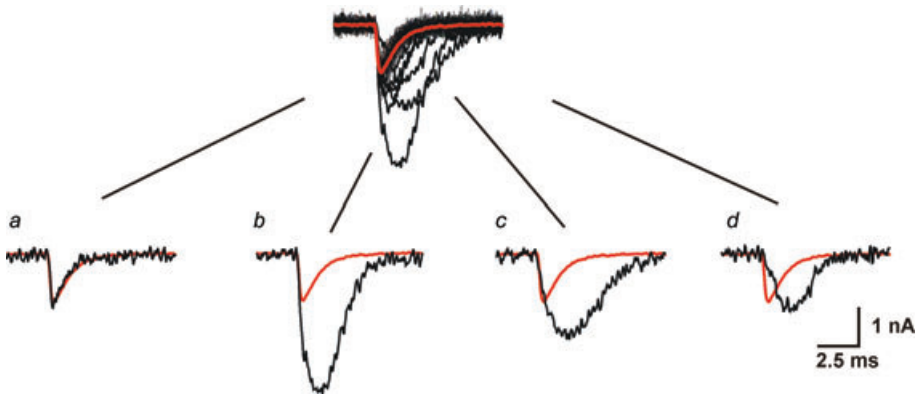

Figure 3. Unusual time courses for mEPCs identified as half-width outliers: examples selected from a Rab3A$^{-/-}$ fibre
A mEPC with a normal half-width (*a*) closely follows the average mEPC, shown in red, whereas three mEPCs with outlier half-widths, *b*–*d*, do not match the average mEPC. The average mEPC trace is obtained by averaging all mEPC traces recorded in the fibre. The examples in *b* and *c* follow the average mEPC initially, but diverge because the current continues past the peak of the average mEPC. In contrast, the example in *d* immediately deviates from the average mEPC with a much reduced slope on the rising phase. The overlay is the same as that shown in Fig. 1*D*.

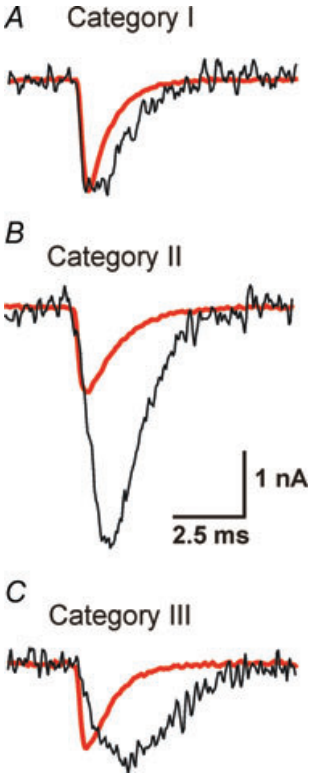

Figure 4. Three categories of long half-width mEPCs can be distinguished based on shape of the rising phase
A, example of a mEPC in Category I, which includes wide mEPCs that rise to a peak with the same time course as the average mEPC, shown in red. *B*, example of a mEPC in Category II, which includes wide mEPCs that initially follow the rising phase of the average mEPC, but continue, and have a 10–90% rise time $\geq$ 0.65 ms. *C*, example of a mEPC in Category III, which includes wide mEPCs that immediately deviate from the average mEPC, and have a rise time $\geq$ 0.65 ms. Note that the average mEPC used for comparision (red trace) is different for each fibre.

pore characteristics, we should observe changes in the amplitude and/or duration of pre-spike feet in Rab3A$^{-/-}$ cells.

We prepared cultures of adrenal chromaffin cells from wild-type and Rab3A$^{-/-}$ animals and recorded amperometric currents evoked by perfusion with 25 mM KCl. Typical ongoing secretory responses evoked by this modest stimulus in a wild-type and a Rab3A$^{-/-}$ cell are shown in Fig. 5*A* and *B*, respectively. We analysed the characteristics of individual amperometric currents as shown in Fig. 5*C*, including spike peak amplitude and half-width, and pre-spike foot amplitude and duration. For every characteristic, a mean value was obtained for each cell, and cell means were averaged to obtain an overall mean. Rab3A loss had no effect on the frequency of events (wild-type, $0.42 \pm 0.04\ s^{-1}$; Rab3A$^{-/-}$, $0.46 \pm 0.05\ s^{-1}$), or the percentage of events with feet (wild-type, $75.5 \pm 1.5\%$; Rab3A$^{-/-}$, $75.5 \pm 1.8\%$). The summary for spike and feet parameters is shown in Table 2. There were no statistically significant differences in main spike amplitude or half-width, and no statistically significant differences in pre-spike foot amplitude or duration.

The lack of effect of loss of Rab3A on parameter means is not surprising, since mean amplitude and half-widths of mEPCs were not altered in Rab3A$^{-/-}$ animals. If the increased occurrence of slow rise mEPCs is due to an increase in abnormal fusion pore openings of small diameter, we should find an increase in the smallest amplitude pre-spike feet. Therefore we examined frequency histograms of pre-spike foot amplitudes for recordings that contained at least 14 feet. Figure 6*A* and *B* shows foot amplitude distributions obtained for a representative wild-type and Rab3A$^{-/-}$ cell, respectively. The distribution for the wild-type cell has 10% in the first

Table 1. Loss of Rab3A increases the incidence of two types of mEPCs with long rise times

Category	Description	WT Total	Rab3A$^{-/-}$ total	WT percent[a]	Rab3A$^{-/-}$ percent[b]	Fold increase[c]
I	Normal 10–90% rise time	86	72	0.58	0.59	1
II	Follows average mEPC initially; 10–90% rise time $\geq$ 0.65 ms	21	49	0.14	0.40	1.9
III	Slowly rising; 10–90% rise time $\geq$0.65 ms	22	82	0.15	0.67	3.5

Miniature endplate currents identified as half-width outliers were further classified based on comparison with the average mEPC for the same fibre. Events with a rising phase that appeared identical to that of the average mEPC were put in Category I; events with a rising phase that followed that of the average mEPC, but continued to rise for a longer time, were put in Category II; events with a rising phase slower than that of the average mEPC were put in Category III. In addition, events in Categories II and III were accepted only if the 10–90% rise time was $\geq$ 0.65 ms. [a]The percentage of wild-type events in categories I–III was determined from: percentage = total/14 704 $\times$ 100; 14 704 is the number of mEPCs recorded in wild-type animals. [b]The percentage of Rab3A$^{-/-}$ events in categories I–III was determined from: percentage = total/12 208 $\times$ 100; 12 208 is the number of mEPCs recorded in Rab3A$^{-/-}$ animals. [c]The fold increase was determined from: (Rab3A$^{-/-}$ percentage – WT percentage)/WT percentage.

bin, 0–2 pA, a mode at the second bin, 2–4 pA, and an extended skew toward high values. The distribution for the Rab3A$^{-/-}$ cell has 52% in the first bin, but otherwise has a similarly skewed shape. The average frequency distribution, obtained by averaging the percentages in each bin across cells, is shown for wild-type and Rab3A$^{-/-}$ cells in Fig. 6*C*. Except for the first bin, the two distributions were very similar. The percentage of events < 2 pA was significantly different between the two groups (Fig. 6*D*, $P < 0.005$, Student's *t* test). Figure 7 shows how amperometric spikes with foot amplitudes < 2 pA (Fig. 7*B* and *C*) compare to a spike with a normal amplitude foot (Fig. 7*A*) and to a spike with no foot (Fig. 7*D*). In summary, loss of Rab3A leads to an increase in the occurrence of extremely small amplitude feet, that are detected with an automated algorithm (Mosharov & Sulzer, 2005), but become apparent only when shown on expanded axes.

We next examined the distribution of foot durations, for pre-spike feet < 2 pA in amplitude, to determine if loss of Rab3A was associated with abnormally long durations. Figure 8*A* shows the foot duration distribution for the same wild-type cell shown in Fig. 6*A*. The largest fraction of events is in the first bin, 0–0.75 ms; no feet are longer than 2.25 ms. In contrast, the foot duration distribution in the Rab3A$^{-/-}$ cell from Fig. 6*B* has a smaller percentage in the first bin, and a number of 'outlier' events $\geq$ 4 ms, which are indicated in gray (Fig. 8*B*). Three examples of events with feet that have amplitude < 2 pA and duration ≥ 4 ms are shown in Fig. 8*C*. We believe these events represent the kinetics of release from a defective fusion pore which is more likely to occur in the absence of Rab3A.

To examine whether the foot duration outliers had qualitatively the same increased occurrence as the half-width outliers observed in neuromuscular junction recordings, we determined the percentage of small amplitude feet with duration ≥ 4 ms for each cell and generated a frequency histogram for wild-type and Rab3A$^{-/-}$ data (Fig. 9*A* and *B*, respectively). These

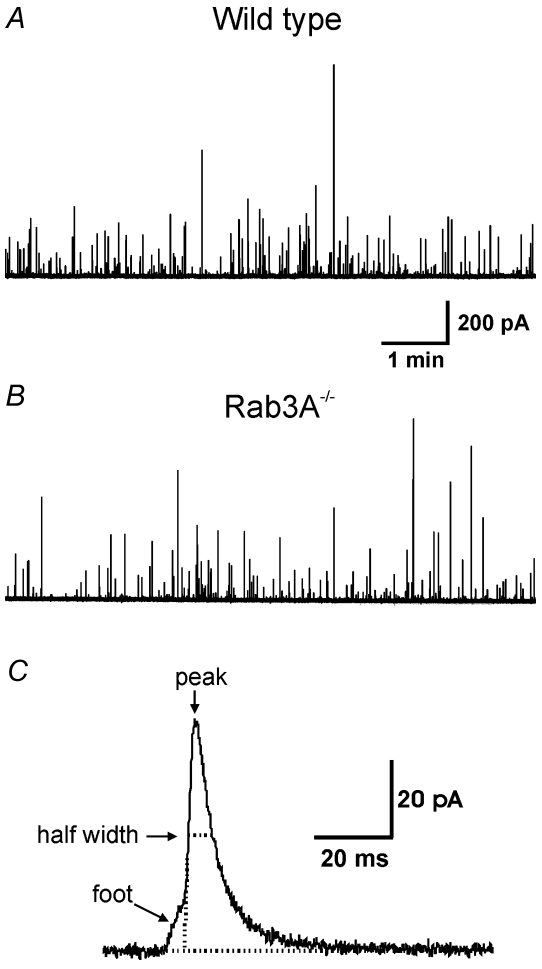

Figure 5. Amperometric currents were elicited by perfusion with 25 mM KCl for 8 min
A and *B*, representative traces recorded in a wild-type and a Rab3A$^{-/-}$ chromaffin cell, respectively. *C*, individual amperometric spike, showing the parameters examined for comparison between wild-type and Rab3A$^{-/-}$ cells. The dotted lines indicating baseline, foot and half-width locations were added by the Quantal Analysis automated detection software (see Methods).

Table 2. Summary of amperometry data from wild-type and Rab3A$^{-/-}$ cells

Genotype	Main spike amplitude (pA)	Main spike half-width (ms)	Pre-spike foot amplitude (pA)	Pre-spike foot duration (ms)	Pre-spike foot charge (fC)	*n*
Wild-type	146.3 ± 14.6	7.4 ± 0.5	7.4 ± 0.6	4.4 ± 0.4	48.0 ± 5.5	31
Rab3A$^{-/-}$	129.9 ± 11.4	7.7 ± 0.6	6.3 ± 0.4	3.8 ± 0.3	40.3 ± 6.3	32

Amperometric events were evoked by perfusion of chromaffin cells with 25 mM KCl for 8 min. Only cells with at least 40 spikes were included in analysis. Each value represents the mean ± S.E.M. of the cell means for *n* cells.

distributions are very similar to those for percentage of mEPCs with abnormal half-widths in wild-type and Rab3A$^{-/-}$ fibres (see Fig. 2*A* and *B*). Figure 9*C* shows the comparison of the cumulative distributions. The percentage of small foot amplitude events ≥ 4 ms was significantly different between wild-type and Rab3A$^{-/-}$ cells ($P < 0.05$, Mann–Whitney U test; $P < 0.05$, Kolmogorov–Smirnov).

Discussion

Loss of Rab3A at the neuromuscular junction leads to an increase in the occurrence of abnormal miniature endplate currents with long half-widths. A key to understanding the function of Rab3A is to determine the mechanism of such abnormal events. The abnormal events have significantly greater total charge than the average mEPC, and a subset of abnormal events have a slow rate of rise. Such changes might be explained by a pool of enlarged vesicles, a subset of which have low transmitter concentration. We focused on a different explanation: that abnormal mEPCs are due to defective fusion pore behaviour. A slowly rising event with a long half-width could be produced by a fusion pore that opens to a small diameter and remains open past the normal time. In support of this idea, we obtained evidence that pre-spike feet in adrenal chromaffin cells are altered in the absence of Rab3A. There is an increase in the smallest amplitude feet, and in this population, there is an increase in those with the longest durations. These changes are consistent with the hypothesis that loss of Rab3A leads to an increased occurrence of small diameter fusion pores that have unusually long open times. Alternatively, loss of Rab3A may cause the fusion pore to flicker, which would reduce the net flux of transmitter.

One interpretation of the correlation between neuromuscular junction and chromaffin cell findings is that Rab3A is involved in the fusion pore mechanism itself. In this scenario, fusion machinery in the absence of Rab3A is more likely to open to a small diameter (or to flicker) and remain open past the normal time. Our hypothesis is detailed in Fig. 10, which shows a comparison of mEPC and amperometric current shapes for different fusion pore behaviours. A normal fusion pore produces a mEPC that is fast and of normal amplitude (Fig. 10*A*); it produces a pre-spike foot that is brief and of normal amplitude (Fig. 10*B*). An abnormal fusion pore that opens to a narrow diameter and remains open produces a mEPC with a slow rise and a long half-width (Fig. 10*C*); it produces a pre-spike foot that is long and of small amplitude (Fig. 10*D*). Below each mEPC and amperometric current is a cartoon depicting the relative loss of vesicle contents during each step of the release process.

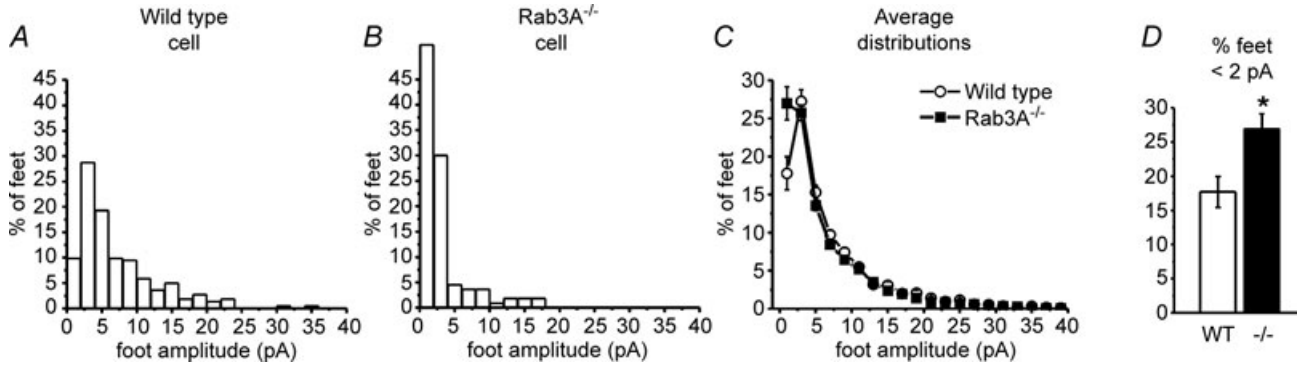

Figure 6. Increased percentage of amperometric spikes with small amplitude feet in Rab3A$^{-/-}$ chromaffin cells

A and *B*, frequency distributions of pre-spike foot amplitudes for a respresentative wild-type cell and Rab3A$^{-/-}$ cell, respectively. *C*, average distributions for wild-type (○) and Rab3A$^{-/-}$ (■) cells, generated by obtaining the mean across cells of the percentage in each bin. *D*, mean percentage of spikes with foot amplitude in the first bin, < 2 pA. $^*P < 0.005$, Student's *t* test, $n = 31$ wild-type cells, 32 Rab3A$^{-/-}$ cells.

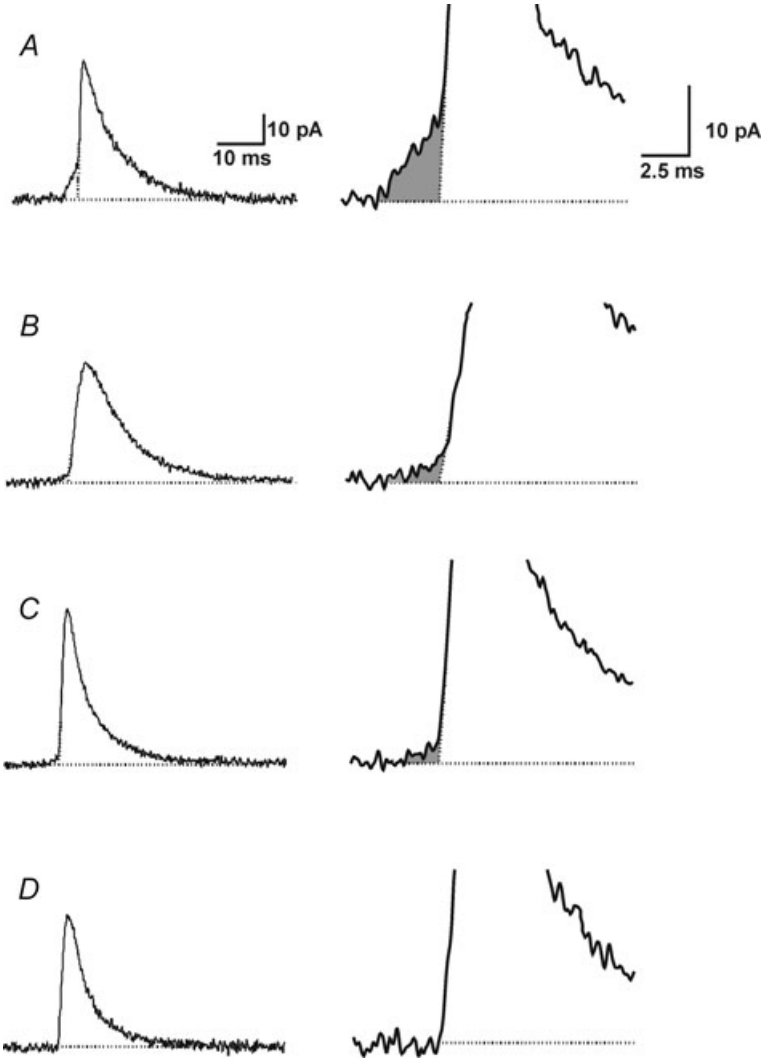

Figure 7. Examples of amperometric spikes with small amplitude pre-spike feet, a normal amplitude foot, and no foot
Traces were selected with similar main spike amplitudes to show a normal amplitude foot, 6.1 pA, 3.3 ms duration (*A*); two small amplitude feet, 1.7 pA, 2.7 ms duration (*B*) and 1.5 pA, 1.8 ms duration (*C*); and a spike with no foot (*D*). The traces on the left and right are the same, shown with different axes. The feet are highlighted in grey on the right only. The dotted lines were added by the Quantal Analysis macro automated detection program (see Methods).

One reason that our data and interpretation are surprising is that Rab3A has been thought of as an activity-dependent regulator of the number of vesicles that fuse, rather than as a shaper of quantal events. An explanation of our data that fits with this role is that Rab3A could regulate (inhibit) the fusion of vesicles with faulty fusion pore machinery. However, more direct regulation of pre-spike feet/fusion pore characteristics by Rab3A is not completely unexpected. Pre-spike foot characteristics are modified by manipulations of SNARE proteins SNAP25, synaptobrevin and syntaxin; as well as the SNARE-interacting proteins synaptotagmin, NSF,

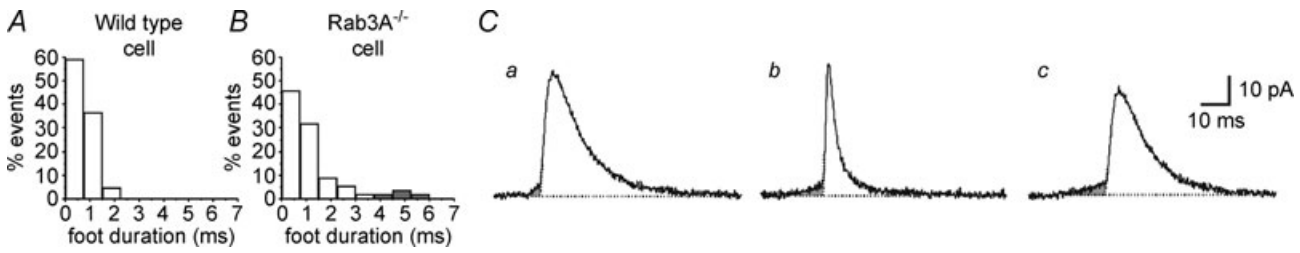

Figure 8. Increased occurrence of long duration feet in Rab3A$^{-/-}$ chromaffin cells
A and *B*, frequency histograms of pre-spike foot durations, for feet < 2 pA, in the same wild-type cell and Rab3A$^{-/-}$ cell shown in Fig. 6*A* and *B*. Outliers, foot durations ≥ 4 ms, are indicated in gray. *C*, examples of amperometric spikes with feet < 2 pA and ≥ 4 ms. Foot parameters 1.8 pA, 4.1 ms (*a*); 1.9 pA, 9.4 ms (*b*); and 1.9 pA, 14.5 ms (*c*).

α-SNAP, SCAMP2, calcium channels, and amisyn (Wang *et al.* 2001; Sorensen *et al.* 2003; Borisovska *et al.* 2005; Constable *et al.* 2005; Han & Jackson, 2006; Ardiles *et al.* 2007; Liao *et al.* 2007). Rab3A interacts with proteins in the SNARE complex (Horikawa *et al.* 1993) as do two of its effectors, rabphilin and RIM (Coppola *et al.* 2001; Tsuboi & Fukuda, 2005; Lee *et al.* 2008). *In vitro* assays of vacuolar fusion show that a rab GTPase is required to concentrate SNARE proteins at sites of fusion (Wang *et al.* 2003). If Rab3A performs a similar role in chromaffin cells, manipulations of Rab3A would affect SNARE protein function, and thereby alter characteristics of pre-spike feet.

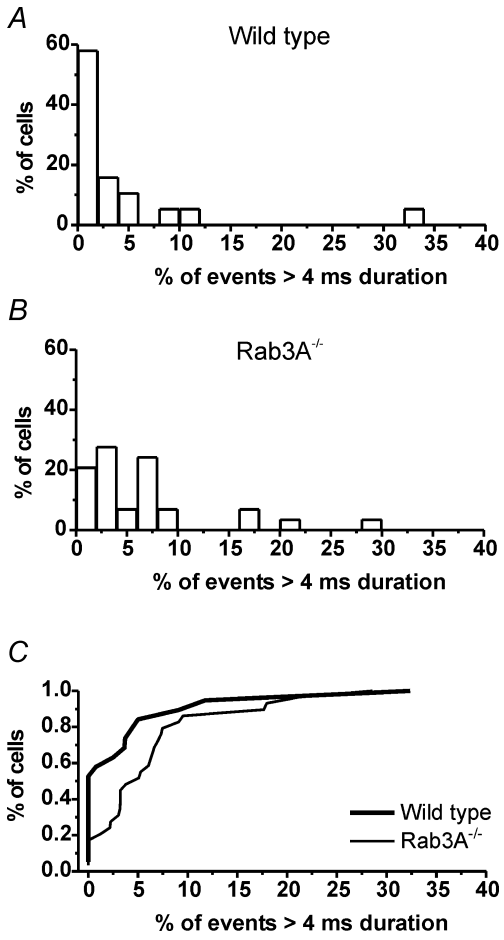

Figure 9. Rab3A$^{-/-}$ chromaffin cells have higher percentages of small amplitude pre-spike feet with long durations
A and *B*, frequency histograms for percentage of feet that are duration outliers, wild-type cells and Rab3A$^{-/-}$ cells, respectively. For each cell, the percentage of duration outliers was determined by counting the number of feet with < 2 pA that had durations $\geq$ than 4 ms, and dividing by the total number of feet < 2 pA. The value of 4 ms was arbitrarily chosen based on examination of foot duration histograms of individual wild-type and Rab3A$^{-/-}$ cells, and determination that for the majority of histograms, there were no values above 4 ms. Only cells with at least 14 feet < 2 pA were included in analysis. The two groups are statistically different, $P < 0.05$, Mann–Whitney *U* test; $P < 0.05$, Kolmogorov–Smirnov. $n = 20$ wild-type cells, 29 Rab3A$^{-/-}$ cells.

Perhaps our most surprising finding is that the abnormal mEPCs have a larger total charge than that of normal mEPCs. The increased charges of slow-rising events, such as those shown in Fig. 3*d* and Fig. 4*C*, are likely to underestimate the increase in ACh released, because the neuromuscular junction is an imperfect detector. The requirement for two acetylcholine molecules to open the channel leads to a supralinear decline in response as ACh concentration is reduced; in addition, acetylcholinesterase will have a greater chance to destroy the slowly released ACh. The larger charge of abnormal mEPCs suggests that normal mEPCs could represent less than complete emptying of the vesicle, due to rapid closure of a fusion pore (Fig. 10*A*). This idea, which rejects the long standing hypothesis that a vesicle's worth of transmitter equals a quantum, clearly requires more than the correlation between abnormal mEPCs and small amplitude pre-spike feet that we report here.

There are ample data based on admittance measurements that transient fusion pore openings occur in neuroendocrine cells and in some nerve terminals. However, none of the events observed are short enough to truncate release during an mEPC, < 5 ms. 'Kiss-and-run' events observed as transient conductance changes derived from admittance recordings in nerve terminals (Klyachko & Jackson, 2002; He *et al.* 2006) have a mean duration of $\sim$300 ms. Transient conductance changes recorded in endocrine cells (Elhamdani *et al.* 2006; Wang *et al.* 2006; Vardjan *et al.* 2007) also have durations in the hundreds of milliseconds. These long duration transient fusion pore openings, which could more aptly be referred to as 'kiss and linger' (Ryan, 2003), are unlikely to shape the majority of fast release events. However, a brief, large conductance opening might be missed with admittance based measurements if the time resolution was low.

A paradigm shift from (a) the mEPC is produced by emptying of vesicle contents during full collapse fusion, to (b) the mEPC is produced by partial release of vesicle contents during a brief fusion pore opening might answer a number of questions about miniature synaptic events that have been previously noted. Several laboratories have described a population of small miniature synaptic events, $\sim$1/10 the size of the normal event (Muniak *et al.* 1982; Csicsaky *et al.* 1988). Giant events, > 2 times the modal value, have also been observed (Molgo & Thesleff, 1982; Alkadhi, 1989). Slowly rising events have been observed in recordings from the frog, rat, mouse and *Torpedo* preparations (Girod *et al.* 1993; Sellin *et al.* 1996). For full fusion to explain these findings requires a wide range of vesicle sizes, filling, or compound fusion (Tremblay *et al.* 1983; Kriebel *et al.* 1990). For example, our results could be attributed to Rab3A-dependent regulation of a pool of vesicles that have higher transmitter content or larger size. However, to account for the slow rises one must also propose that these vesicles are released

distantly from receptors. A fusion pore mechanism more concisely accounts for a wide range of mEPC sizes and shapes. A similar conclusion was reached in a review by Rahamimoff and Fernandez, who stated that 'the duration of transient fusion would be one of the determinants of the size of the quantum' (Rahamimoff & Fernandez, 1997).

The equivalence of miniature synaptic events and full release of vesicle contents was based in part on the observation that the miniature event at the frog neuromuscular junction was matched by application of 10 000 molecules of iontophoretically applied ACh (Kuffler & Yoshikami, 1975), which is the same as the amount per vesicle determined biochemically (Miledi *et al.* 1982). However, the biochemical measurements were divided by an estimate of the number of vesicles per endplate, which in turn was based on an estimate of the number of endplates in the muscle sample. A more direct measure of the amount of ACh per vesicle was obtained in studies of *Torpedo* electric organ. The vesicles in a purified preparation were subjected to electron microscopy and counted. Using that number as the denominator for the biochemically measured ACh concentration, the number of molecules per vesicle was 200 000 (Ohsawa *et al.* 1979). Vesicles from *Torpedo* are larger than those of the frog or mammalian neuromuscular junction (84 nm *versus* 50 nm diameter), but the amount of ACh packaged at the same concentration in a 50 nm vesicle would be around 40 000 molecules. Therefore, despite general acceptance that synaptic vesicles contain 10 000 molecules, it remains a possibility that 10 000 molecules represent only partial release.

There is a quantitative problem with our interpretation that normal mEPCs are shaped by fusion pore closure. If the fusion pore behaves like an ion channel, its open time histogram should have an exponential shape. This is what we observe for the histograms of durations for small amplitude feet in chromaffin cells (Fig. 8; see also Chow *et al.* 1992; Zhou *et al.* 1996). However, the mEPC half-width histogram has a normal/Gaussian shape (except for the abnormal mEPCs). If the normal mEPC is limited by closure of a fusion pore, there must be an

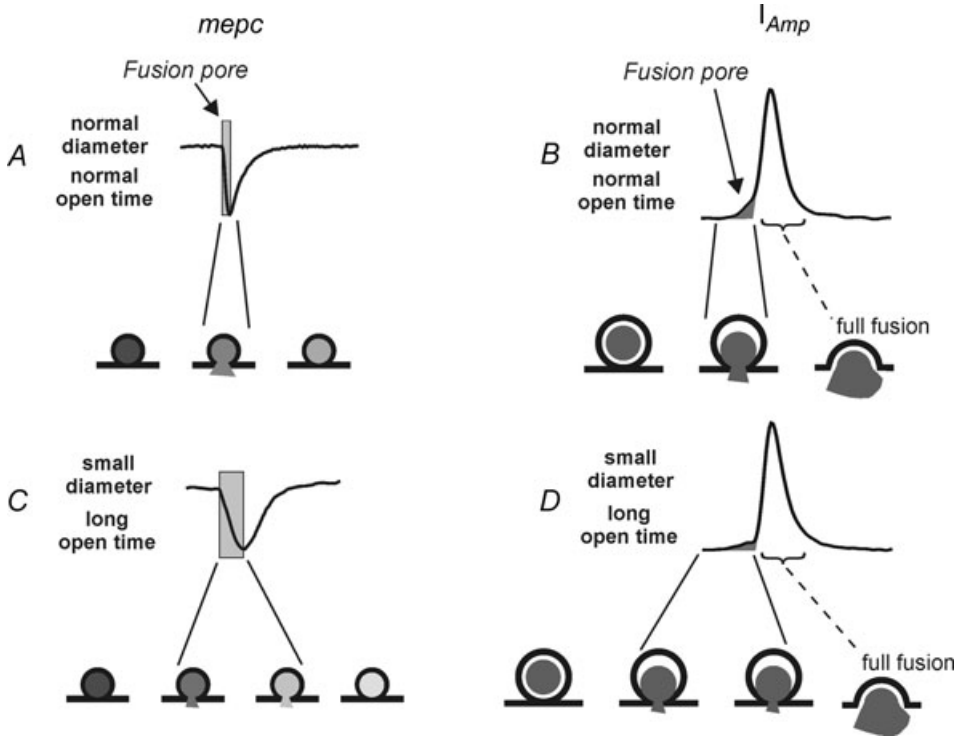

Figure 10. The effect of fusion pore behaviour on mEPCs and amperometric currents (I_{Amp})
A, a large diameter fusion pore, open for a brief time (shaded area), produces a normal mEPC. The fusion pore/vesicle cartoons below show that when the fusion pore closes, some transmitter remains in the vesicle. *B*, idealized amperometric current (I_{Amp}) produced by a fusion pore with the same relative characteristics as in *A*. *C*, a small diameter fusion pore, open for a long time, produces a slowly rising mEPC with a wide half-width. A greater fraction of the vesicle contents is released than in *A*. *D*, idealized amperometric current produced by a fusion pore with the same relative characteristics as in *C*. Note that for I_{Amp}, the fusion pore determines the shape of the pre-spike foot. The amount of catecholamine released during the foot is a small fraction of the total contained in the vesicle. Therefore changes in foot characteristics do not necessarily affect those of the main spike, when the major part of the vesicle content is released through a wide fusion pore or full collapse fusion.

additional regulatory control so that the fusion pore no longer behaves in a probabilistic manner.

We are not the first to suggest our data support the idea that transmitter is released from nerve terminals via transient opening of a fusion pore. In amperometric recordings from dopaminergic neurons cultured from the ventral midbrain (Staal *et al.* 2004), two types of events were observed: simple events comprised of single peaks with half-widths < 1 ms, and complex events made of multiple peaks. Since subsequent peaks in a complex event were smaller than the first peak, it was concluded that complex events were made of flickers of a fusion pore, with each flicker causing partial release. Simple events, which had less charge than the complex events, were interpreted as a single opening and closing of a fusion pore. Pawlu *et al.* (2004) observed that uniquantal glutamate currents recorded extracellularly from the *Drosophila* larval neuromuscular junction usually displayed a hump or plateau on the decay phase. They modelled this shape with a narrow fusion pore that expanded after a delay, and showed that the relative size of the hump could be altered by changing extracellular calcium, increasing expression of synaptotagmin IV, or deleting endophilin. Finally, He *et al.* (2006, Supplemental Data) observed a correlation between the fraction of fusion pores of small conductance detected with admittance measurements, and the fraction of postsynaptically recorded miniature excitatory synaptic currents with slow rise times, which suggests the latter could be caused by release through an abnormally small diameter fusion pore.

There is one piece of evidence that appears to negate our hypothesis that mEPCs are due to transient opening of a fusion pore. At the calyx of Held synapse, Wu *et al.* (2007) aligned over 2.6 million miniature synaptic current traces with a simultaneous measurement of capacitance, and the average capacitance increase was the size expected for fusion of one vesicle. If transient fusion was the dominant mode, the mean capacitance change should have been less than expected, or should not have been persistent. Therefore at the calyx of Held, spontaneous miniature synaptic events appear to be due to full collapse fusion. Our hypothesis may still hold if full fusion was induced by the raised intracellular calcium used to increase miniature synaptic current frequency. Alternatively, the release process at the calyx of Held, where miniature synaptic current amplitudes have a skewed distribution, may differ from that at the neuromuscular junction, where current amplitudes have a Gaussian distribution.

A less controversial interpretation of our results is that Rab3A regulates the trafficking and/or fusion of a pool of vesicles characterized by abnormal fusion pores and larger sizes. There is precedence for regulation by Rab3A of vesicles with unique release characteristics. In hippocampal autaptic cultures, loss of Rab3A selectively affects a pool of vesicles with a higher calcium sensitivity (Schluter *et al.* 2006). The rarity of abnormal mEPCs at the neuromuscular junction, and the small magnitude of the changes in chromaffin cells, preclude looking for large vesicles with electron microscopy. It should be noted that a dramatic increase in abnormal, giant miniature end-plate potentials at neuromuscular junctions treated with 4-aminoquinolone was not accompanied by any change in vesicle size distributions (Pecot-Dechavassine & Molgo, 1982).

In conclusion, our data are the first to show that the presence of Rab3A is important for shaping individual quantal events, and for shaping the distributions of event characteristics. We propose that Rab3A either regulates the fusion pore directly, or controls the fusion of vesicles based on fusion pore characteristics. Although these two interpretations have radically different implications, both are consistent with the idea that Rab3A, in addition to its well-established role in regulating release probability, has a role in regulating synaptic strength through changes in quantal shape and size.

References

Albillos A, Dernick G, Horstmann H, Almers W, Alvarez de Toledo G & Lindau M (1997). The exocytotic event in chromaffin cells revealed by patch amperometry. *Nature* **389**, 509–512.

Ales E, Tabares L, Poyato JM, Valero V, Lindau M & Alvarez de Toledo G (1999). High calcium concentrations shift the mode of exocytosis to the kiss-and-run mechanism. *Nat Cell Biol* **1**, 40–44.

Alkadhi KA (1989). Giant miniature end-plate potentials at the untreated and emetine-treated frog neuromuscular junction. *J Physiol* **412**, 475–491.

Ardiles AO, Gonzalez-Jamett AM, Maripillan J, Naranjo D, Caviedes P & Cardenas AM (2007). Calcium channel subtypes differentially regulate fusion pore stability and expansion. *J Neurochem* **103**, 1574–1581.

Becherer U, Guatimosim C & Betz W (2001). Effects of staurosporine on exocytosis and endocytosis at frog motor nerve terminals. *J Neurosci* **21**, 782–787.

Borisovska M, Zhao Y, Tsytsyura Y, Glyvuk N, Takamori S, Matti U, Rettig J, Sudhof T & Bruns D (2005). v-SNAREs control exocytosis of vesicles from priming to fusion. *EMBO J* **24**, 2114–2126.

Castillo PE, Janz R, Sudhof TC, Tzounopoulos T, Malenka RC & Nicoll RA (1997). Rab3A is essential for mossy fibre long-term potentiation in the hippocampus. *Nature* **388**, 590–593.

Chow RH, von Ruden L & Neher E (1992). Delay in vesicle fusion revealed by electrochemical monitoring of single secretory events in adrenal chromaffin cells. *Nature* **356**, 60–63.

Coleman WL, Bill CA & Bykhovskaia M (2007). Rab3a deletion reduces vesicle docking and transmitter release at the mouse diaphragm synapse. *Neuroscience* **148**, 1–6.

Constable JR, Graham ME, Morgan A & Burgoyne RD (2005). Amisyn regulates exocytosis and fusion pore stability by both syntaxin-dependent and syntaxin-independent mechanisms. *J Biol Chem* **276**, 32756–32762.

Coppola T, Magnin-Luthi S, Perret-Menoud V, Gattesco S, Schiavo G & Regazzi R (2001). Direct interaction of the Rab3 effector RIM with Ca^{2+} channels, SNAP-25, and synaptotagmin. *J Biol Chem* **276**, 32756–32762.

Csicsaky M, Wiegand H, Uhlig S, Lohmann H & Papadopoulos R (1988). Miniature endplate potentials as a tool in neurotoxicology. *Toxicology* **49**, 121–129.

Darchen F, Zahraoui A, Hammel F, Monteils MP, Tavitian A & Scherman D (1990). Association of the GTP-binding protein Rab3A with bovine adrenal chromaffin granules. *Proc Natl Acad Sci U S A* **87**, 5692–5696.

Dickman DK, Horne JA, Meinertzhagen IA & Schwarz TL (2005). A slowed classical pathway rather than kiss-and-run mediates endocytosis at synapses lacking synaptojanin and endophilin. *Cell* **123**, 521–533.

Elhamdani A, Azizi F & Artalejo CR (2006). Double patch clamp reveals that transient fusion (kiss-and-run) is a major mechanism of secretion in calf adrenal chromaffin cells: high calcium shifts the mechanism from kiss-and-run to complete fusion. *J Neurosci* **26**, 3030–3036.

Fischer von Mollard G, Mignery GA, Baumert M, Perin MS, Hanson TJ, Burger PM, Jahn R & Sudhof TC (1990). rab3 is a small GTP-binding protein exclusively localized to synaptic vesicles. *Proc Natl Acad Sci U S A* **87**, 1988–1992.

Fulop T & Smith C (2006). Physiological stimulation regulates the exocytic mode through calcium activation of protein kinase C in mouse chromaffin cells. *Biochem J* **399**, 111–119.

Geppert M, Bolshakov VY, Siegelbaum SA, Takei K, De Camilli P, Hammer RE & Sudhof TC (1994). The role of Rab3A in neurotransmitter release. *Nature* **369**, 493–497.

Girod R, Correges P, Jacquet J & Dunant Y (1993). Space and time characteristics of transmitter release at the nerve–electroplaque junction of *Torpedo*. *J Physiol* **471**, 129–157.

Han X & Jackson MB (2006). Structural transitions in the synaptic SNARE complex during Ca^{2+}-triggered exocytosis. *J Cell Biol* **172**, 281–293.

He L, Wu XS, Mohan R & Wu LG (2006). Two modes of fusion pore opening revealed by cell-attached recordings at a synapse. *Nature* **444**, 102–105.

Heuser JE, Reese TS, Dennis MJ, Jan Y, Jan L & Evans L (1979). Synaptic vesicle exocytosis captured by quick freezing and correlated with quantal transmitter release. *J Cell Biol* **81**, 275–300.

Hirsh JK, Searl TJ & Silinsky EM (2002). Regulation by Rab3A of an endogenous modulator of neurotransmitter release at mouse motor nerve endings. *J Physiol* **545**, 337–343.

Horikawa HP, Saisu H, Ishizuka T, Sekine Y, Tsugita A, Odani S & Abe T (1993). A complex of rab3A, SNAP-25, VAMP/synaptobrevin-2 and syntaxins in brain presynaptic terminals. *FEBS Lett* **330**, 236–240.

Huang YY, Zakharenko SS, Schoch S, Kaeser PS, Janz R, Sudhof TC, Siegelbaum SA & Kandel ER (2005). Genetic evidence for a protein-kinase-A-mediated presynaptic component in NMDA-receptor-dependent forms of long-term synaptic potentiation. *Proc Natl Acad Sci U S A* **102**, 9365–9370.

Kapfhamer D, Valladares O, Sun Y, Nolan PM, Rux JJ, Arnold SE, Veasey SC & Bucan M (2002). Mutations in Rab3a alter circadian period and homeostatic response to sleep loss in the mouse. *Nat Genet* **32**, 290–295.

Klyachko VA & Jackson MB (2002). Capacitance steps and fusion pores of small and large-dense-core vesicles in nerve terminals. *Nature* **418**, 89–92.

Kriebel ME, Vautrin J & Holsapple J (1990). Transmitter release: prepackaging and random mechanism or dynamic and deterministic process. *Brain Res Brain Res Rev* **15**, 167–178.

Kuffler SW & Yoshikami D (1975). The number of transmitter molecules in a quantum: an estimate from iontophoretic application of acetylcholine at the neuromuscular synapse. *J Physiol* **251**, 465–482.

Lee JD, Chang YF, Kao FJ, Kao LS, Lin CC, Lu AC, Shyu BC, Chiou SH & Yang DM (2008). Detection of the interaction between SNAP25 and rabphilin in neuroendocrine PC12 cells using the FLIM/FRET technique. *Microsc Res Tech* **71**, 26–34.

Leenders AG, da Silva FH, Ghijsen WE & Verhage M (2001). Rab3a is involved in transport of synaptic vesicles to the active zone in mouse brain nerve terminals. *Mol Biol Cell* **12**, 3095–3102.

Liao H, Ellena J, Liu L, Szabo G, Cafiso D & Castle D (2007). Secretory carrier membrane protein SCAMP2 and phosphatidylinositol 4,5-bisphosphate interactions in the regulation of dense core vesicle exocytosis. *Biochemistry* **46**, 10909–10920.

Magrassi L, Purves D & Lichtman JW (1987). Fluorescent probes that stain living nerve terminals. *J Neurosci* **7**, 1207–1214.

Miledi R, Molenaar PC & Polak RL (1982). Free and bound acetylcholine in frog muscle. *J Physiol* **333**, 189–199.

Molgo J & Thesleff S (1982). 4-Aminoquinoline-induced 'giant' miniature endplate potentials at mammalian neuromuscular junctions. *Proc R Soc Lond B Biol Sci* **214**, 229–244.

Mosharov EV & Sulzer D (2005). Analysis of exocytotic events recorded by amperometry. *Nat Methods* **2**, 651–658.

Muniak CG, Kriebel ME & Carlson CG (1982). Changes in MEPP and EPP amplitude distributions in the mouse diaphragm during synapse formation and degeneration. *Brain Res* **281**, 123–138.

Ohsawa K, Dowe GH, Morris SJ & Whittaker VP (1979). The lipid and protein content of cholinergic synaptic vesicles from the electric organ of *Torpedo marmorata* purified to constant composition: implications for vesicle structure. *Brain Res* **161**, 447–457.

Pawlu C, DiAntonio A & Heckmann M (2004). Postfusional control of quantal current shape. *Neuron* **42**, 607–618.

Pecot-Dechavassine M & Molgo J (1982). Attempt to detect morphological correlates for the giant miniature end plate potentials induced by 4 amino quinoline. *Biol Cell (Paris)* **46**, 93–96.

Rahamimoff R & Fernandez JM (1997). Pre- and postfusion regulation of transmitter release. *Neuron* **18**, 17–27.

Regazzi R, Kikuchi A, Takai Y & Wollheim CB (1992). The small GTP-binding proteins in the cytosol of insulin-secreting cells are complexed to GDP dissociation inhibitor proteins. *J Biol Chem* **267**, 17512–17519.

Ryan TA (2003). Kiss-and-run, fuse-pinch-and-linger, fuse-and-collapse: the life and times of a neurosecretory granule. *Proc Natl Acad Sci U S A* **100**, 2171–2173.
Salminen A & Novick PJ (1987). A ras-like protein is required for a post-Golgi event in yeast secretion. *Cell* **49**, 527–538.
Schluter OM, Basu J, Sudhof TC & Rosenmund C (2006). Rab3 superprimes synaptic vesicles for release: implications for short-term synaptic plasticity. *J Neurosci* **26**, 1239–1246.
Schluter OM, Schmitz F, Jahn R, Rosenmund C & Sudhof TC (2004). A complete genetic analysis of neuronal Rab3 function. *J Neurosci* **24**, 6629–6637.
Schoch S, Castillo PE, Jo T, Mukherjee K, Geppert M, Wang Y, Schmitz F, Malenka RC & Sudhof TC (2002). RIM1α forms a protein scaffold for regulating neurotransmitter release at the active zone. *Nature* **415**, 321–326.
Segev N & Botstein D (1987). The ras-like yeast YPT1 gene is itself essential for growth, sporulation, and starvation response. *Mol Cell Biol* **7**, 2367–2377.
Sellin LC, Molgo J, Tornquist K, Hansson B & Thesleff S (1996). On the possible origin of giant or slow-rising miniature end-plate potentials at the neuromuscular junction. *Pflugers Arch* **431**, 325–334.
Sons MS & Plomp JJ (2006). Rab3A deletion selectively reduces spontaneous neurotransmitter release at the mouse neuromuscular synapse. *Brain Res* **1089**, 126–134.
Sorensen JB, Nagy G, Varoqueaux F, Nehring RB, Brose N, Wilson MC & Neher E (2003). Differential control of the releasable vesicle pools by SNAP-25 splice variants and SNAP-23. *Cell* **114**, 75–86.
Staal RG, Mosharov EV & Sulzer D (2004). Dopamine neurons release transmitter via a flickering fusion pore. *Nat Neurosci* **7**, 341–346.
Thakker-Varia S, Alder J, Crozier RA, Plummer MR & Black IB (2001). Rab3A is required for brain-derived neurotrophic factor-induced synaptic plasticity: transcriptional analysis at the population and single-cell levels. *J Neurosci* **21**, 6782–6790.
Thiagarajan R, Tewolde T, Li Y, Becker PL, Rich MM & Engisch KL (2004). Rab3A negatively regulates activity-dependent modulation of exocytosis in bovine adrenal chromaffin cells. *J Physiol* **555**, 439–457.
Tremblay JP, Laurie RE & Colonnier M (1983). Is the MEPP due to the release of one vesicle or to the simultaneous release of several vesicles at one active zone? *Brain Res* **287**, 299–314.
Tsuboi T & Fukuda M (2005). The C2B domain of rabphilin directly interacts with SNAP-25 and regulates the docking step of dense core vesicle exocytosis in PC12 cells. *J Biol Chem* **280**, 39253–39259.
Vardjan N, Stenovec M, Jorgacevski J, Kreft M & Zorec R (2007). Subnanometer fusion pores in spontaneous exocytosis of peptidergic vesicles. *J Neurosci* **27**, 4737–4746.
Wang CT, Bai J, Chang PY, Chapman ER & Jackson MB (2006). Synaptotagmin-Ca^{2+} triggers two sequential steps in regulated exocytosis in rat PC12 cells: fusion pore opening and fusion pore dilation. *J Physiol* **570**, 295–307.
Wang CT, Grishanin R, Earles CA, Chang PY, Martin TF, Chapman ER & Jackson MB (2001). Synaptotagmin modulation of fusion pore kinetics in regulated exocytosis of dense-core vesicles. *Science* **294**, 1111–1115.
Wang L, Merz AJ, Collins KM & Wickner W (2003). Hierarchy of protein assembly at the vertex ring domain for yeast vacuole docking and fusion. *J Cell Biol* **160**, 365–374.
Wichmann H, Hengst L & Gallwitz D (1992). Endocytosis in yeast: evidence for the involvement of a small GTP-binding protein (Ypt7p). *Cell* **71**, 1131–1142.
Wightman RM, Jankowski JA, Kennedy RT, Kawagoe KT, Schroeder TJ, Leszczyszyn DJ, Near JA, Diliberto EJ Jr & Viveros OH (1991). Temporally resolved catecholamine spikes correspond to single vesicle release from individual chromaffin cells. *Proc Natl Acad Sci U S A* **88**, 10754–10758.
Wu XS, Xue L, Mohan R, Paradiso K, Gillis KD & Wu LG (2007). The origin of quantal size variation: vesicular glutamate concentration plays a significant role. *J Neurosci* **27**, 3046–3056.
Zhou Z, Misler S & Chow RH (1996). Rapid fluctuations in transmitter release from single vesicles in bovine adrenal chromaffin cells. *Biophys J* **70**, 1543–1552.

Acknowledgements

We thank Maja Bucan for providing $Rab3A^{+/-}$ breeders and Shuzhang Yang for the genotyping protocol and initial genotyping, and Martin Pinter and Eugene Mosharov for custom software. This work was supported by NIMH R01 MH064744, NIH P01 NS057228 (T. C. Cope, PI), and Wright State University start up funds.

Author's present address

T. Tewolde: Neuroscience Institute, Morehouse School of Medicine, Atlanta, GA 30310, USA.